

# Qubit-mediated energy transfer between thermal reservoirs: Beyond the Markovian master equation

Dvira Segal

*Chemical Physics Theory Group, Department of Chemistry, University of Toronto, 80 Saint George St., Toronto, Ontario, Canada M5S 3H6*  
(Received 22 March 2013; revised manuscript received 5 May 2013; published 21 May 2013)

We study qubit-mediated energy transfer between two electron reservoirs by adopting a numerically exact influence functional path-integral method. This nonperturbative technique allows us to study the system's dynamics beyond the weak coupling limit. Our simulations for the energy current indicate that perturbative-Markovian master equation predictions significantly deviate from exact numerical results already at intermediate coupling  $\pi\rho\alpha_{j,j'} \gtrsim 0.4$ , where  $\rho$  is the metal (Fermi sea) density of states, taken as a constant, and  $\alpha_{j,j'}$  is the scattering potential energy of electrons, between the  $j$  and  $j'$  states. Perturbative Markovian master equation techniques should be therefore used with caution beyond the strictly weak subsystem-bath coupling limit, especially when a quantitative knowledge of transport characteristics is desired.

DOI: [10.1103/PhysRevB.87.195436](https://doi.org/10.1103/PhysRevB.87.195436)

PACS number(s): 05.60.-k, 44.10.+i, 73.23.-b

## I. INTRODUCTION

Quantum impurity models, including a subsystem interacting with a reservoir, were proven useful in describing and predicting many physical phenomena. The spin-boson model,<sup>1</sup> representing the dynamics of a single charge on two states coupled to a dissipative bath, e.g., a solvent, exhibits rich phenomenology, including various phase transitions.<sup>2</sup> It is relevant for modeling charge transfer reactions in biological systems,<sup>2</sup> photosynthesis,<sup>3</sup> the Kondo problem for magnetic impurities,<sup>4</sup> and quantum information processing in superconducting Josephson tunneling junction qubits<sup>5</sup> or nitrogen-vacancy centers in diamonds.<sup>6</sup> A variant of the spin-boson model is the spin-fermion model, where a qubit, referred to as a spin or a two-level system, interacts with a metallic-fermionic environment. This model is also related to the Kondo model,<sup>4</sup> only lacking direct coupling of the reservoir degrees of freedom to spin-flip processes. The generalization of the equilibrium spin-fermion model, to include more than one Fermi bath, provides a minimal setting for the study of dissipation and decoherence effects under the influence of an out-of-equilibrium environment.<sup>7-10</sup>

In this work, we use the two-bath spin-fermion model and investigate the energy exchange between two metals, mediated by the excitation or relaxation of a nonlinear quantum system, a qubit. For a scheme of this setup, see Fig. 1. Physically, our model can describe the process of radiative heat transfer between metals,<sup>11-13</sup> and it can be realized within a superconducting Josephson junction circuit.<sup>10,14,15</sup> We simulate the energy current characteristics of the nonequilibrium spin-fermion model in a large parameter range of coupling strengths by means of an influence-functional path-integral (INFPI) technique developed by the authors of Refs. 16 and 17. This numerically exact method is built about the basic observation that in out-of-equilibrium (and/or finite temperature) situations bath correlations have a finite range, allowing for their truncation beyond a memory time dictated by the voltage-bias and the temperature.<sup>8,9,18</sup> Taking advantage of this fact, an iterative-deterministic time-evolution scheme can be developed where convergence with respect to the memory length can in principle be reached.<sup>16,17</sup>

Our main objective here is to explore qubit-mediated energy current characteristics beyond standard perturbative methods. Particularly, we would like to find when the Golden-Rule-type (second-order perturbation theory) Markovian master equation method provides a correct, quantitative, or qualitative, description of the exact behavior. This task is important since master equation tools have been extensively adopted for studying problems in charge, spin, and energy transfer phenomenology in quantum dots and molecular junctions, see, for example, Refs. 13,19-28.

The plan of the paper is as follows. In Sec. II we present the nonequilibrium spin-fermion model. We provide expressions for observables of interest in Sec. III. The two methods confronted, INFPI and the perturbative Markovian master equation, are discussed in Sec. IV, with the results included in Sec. V. Section VI concludes. For simplicity, we use the conventions  $\hbar \equiv 1$ , electron charge  $e \equiv 1$ , and Boltzmann constant  $k_B = 1$ .

## II. MODEL

The system of interest comprises of two metallic leads,  $\nu = L, R$ , prepared at different temperatures but at the same chemical potential. These metals are connected indirectly by a nonlinear quantum unit, a two-level subsystem. The Hamiltonian includes three contributions

$$H = H_S + H_F + V, \quad (1)$$

where

$$\begin{aligned} H_S &= \Delta\sigma_z, \\ H_F &= H_L + H_R, \quad H_\nu = \sum_j \epsilon_j c_{\nu,j}^\dagger c_{\nu,j}, \\ V &= V_L + V_R, \quad V_\nu = \sigma_x \sum_{j,j'} \alpha_{\nu,j;j'} c_{\nu,j}^\dagger c_{\nu,j'}. \end{aligned} \quad (2)$$

Here,  $\sigma_{x,y,z}$  represent the Pauli matrices. The subsystem  $H_S$  includes two states,  $|0\rangle$  and  $|1\rangle$ , with a tunneling splitting  $2\Delta$ . It can be realized within a nonlinear resonator mode, or it can represent an impurity in a solid-state environment. This subsystem interacts with two fermionic reservoirs, comprised

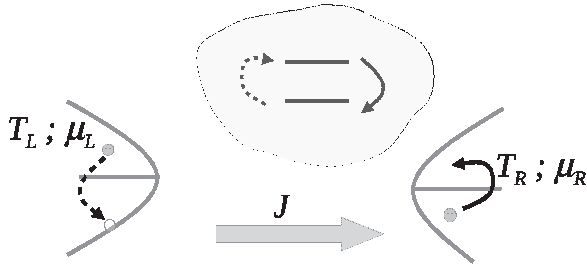


FIG. 1. A schematic representation of our model system. Electron transfer between the metals is blocked, but energy current is flowing through an excitation or deexcitation of the intermediate anharmonic (two-state) quantum system. The curved arrows represent energy transfer processes between the leads and the intermediating subsystem. In our work here we set  $\mu_L = \mu_R$  and take  $T_L > T_R$ .

in  $H_F$ , where  $c_{\nu,j}^\dagger$  ( $c_{\nu,j}$ ) creates (annihilates) an electron at the  $\nu = L, R$  metal lead with momentum  $j$ , disregarding the electron spin degree of freedom. The qubit-metal interaction term  $V$  couples scattering events within each metal to transitions within the subsystem. For simplicity, we assume that the coupling constants  $\alpha_\nu$  are energy independent and real numbers. Note that we do not allow for charge transfer processes between the two metals, assuming the tunneling barrier is high. However, energy is transferred between the two metals, mediated by the excitation of the intermediate nonlinear quantum system, see Fig. 1. Using the Hamiltonian form (2), the subsystem dynamics and the energy current can be readily attained within a Markovian master equation, as we explain in Sec. IV B

The Hamiltonian (2) can be transformed into the standard spin-fermion model of zero energy spacing with a unitary transformation

$$U^\dagger \sigma_z U = \sigma_x, \quad U^\dagger \sigma_x U = \sigma_z, \quad (3)$$

where  $U = \frac{1}{\sqrt{2}}(\sigma_x + \sigma_z)$ . The transformed Hamiltonian  $H_{SF} = U^\dagger H U$  includes a  $\sigma_z$ -type electron-spin coupling

$$H_{SF} = \Delta \sigma_x + \sum_{\nu,j} \epsilon_j c_{\nu,j}^\dagger c_{\nu,j} + \sigma_z \sum_{\nu,j,j'} \alpha_{\nu,j;j'} c_{\nu,j}^\dagger c_{\nu,j'}. \quad (4)$$

In this representation, the dynamics can be conveniently simulated using INFPI; a brief discussion is included in Sec. IV A.

### III. OBSERVABLES

We assume a factorized initial state with the total density matrix  $\rho(0) = \rho_S(0) \otimes \rho_F$ . Here  $\rho_S$  denotes the reduced density matrix (RDM) of the subsystem. The reservoirs' density matrix at time  $t = 0$  is given by  $\rho_F = \rho_L \otimes \rho_R$ , and these states are canonical,  $\rho_\nu = e^{-\beta_\nu(H_\nu - \mu_\nu N_\nu)} / \text{Tr}_\nu[e^{-\beta_\nu(H_\nu - \mu_\nu N_\nu)}]$ . Here we trace over the  $\nu$  reservoirs' degrees of freedom. In our simulations below we take  $\mu_L = \mu_R$ , but assume different initial temperatures  $T_L \neq T_R$ . We refer to this setup as a “nonequilibrium environment” since the two reservoirs are prepared in different states. At time  $t = 0$  we put into contact the two Fermi baths through the quantum subsystem and follow

the evolution of the RDM and the energy current, to steady state. Since the energy current through the subsystem is driven by a temperature bias, we can also refer to it as a “heat current.”

The time evolution of the RDM is obtained by tracing  $\rho$  over the fermionic reservoirs' degrees of freedom ( $\text{Tr}_F = \text{Tr}_L \text{Tr}_R$ ),

$$\rho_S(t) = \text{Tr}_F[e^{-iHt} \rho(0) e^{iHt}]. \quad (5)$$

The definition of the energy current operator is more subtle,<sup>29,30</sup> as different-plausible choices provide distinct results in the short time limit. At long time, in the steady-state limit, these definitions yield the same value. Here, we follow the analysis of the authors of Ref. 29, and define the energy current operator, e.g., at the left contact, as

$$\hat{J}_L = \frac{i}{2} [H_L - H_S, V_L]. \quad (6)$$

The current is defined positive when flowing from  $L$  bath to the subsystem. This expression can be derived by assuming that there is an operator continuity equation for the energy density operator, and by partitioning the interaction energy between the three “sites,” the  $L$  and  $R$  baths, and the subsystem.<sup>29</sup> In the steady state the expectation value of the time derivative of the interaction is zero

$$\text{Tr} \left[ \rho \frac{\partial V_L}{\partial t} \right] \equiv \left\langle \frac{\partial V_L}{\partial t} \right\rangle = i \langle [H_S + H_L, V_L] \rangle = 0, \quad (7)$$

and we reach the relation

$$\langle [H_S, V_L] \rangle = \langle [V_L, H_L] \rangle, \quad (8)$$

where we have assumed that  $[V_L, V_R] = 0$ . We can now identify the averaged energy current, in the long time limit, as

$$\langle J_L \rangle \equiv \text{Tr}_S \text{Tr}_F [\hat{J}_L \rho(t)] = -i \langle [H_S, V_L] \rangle. \quad (9)$$

Alternatively, one can derive this expression from the Heisenberg time-evolution relation for the  $L$  bath energy operator

$$\frac{dH_L}{dt} = i[H, H_L] = i[V_L, H_L]. \quad (10)$$

The average energy current is given by the rate of energy change

$$\langle J_L \rangle = - \left\langle \frac{dH_L}{dt} \right\rangle, \quad (11)$$

with the minus sign included to accommodate the sign convention for the current. Using the steady-state result (8), we immediately retrieve Eq. (9).

We now evaluate the relevant commutator, using the Hamiltonian (2),

$$[H_S, V_L] = 2i \Delta \sigma_y \sum_{l,l'} \alpha_{L,l;L,l'} c_{L,l}^\dagger c_{L,l'}. \quad (12)$$

The energy current then reduces to

$$\langle J_L \rangle = 2\Delta \text{Tr}_S [\sigma_y \text{Tr}_F [A_L \rho(t)]], \quad (13)$$

which can be conveniently expressed in terms of subsystem operators as

$$\langle J_L \rangle = 2\Delta \text{Tr}_S [\sigma_y A_S(t)]. \quad (14)$$

Here we defined a bath operator, quadratic in the creation and annihilation operators,

$$A_L \equiv \sum_{l,l'} \alpha_{L,l;l',l'} c_{L,l}^\dagger c_{L,l'}, \quad (15)$$

and the related-reduced subsystem operator

$$\begin{aligned} A_S(t) &\equiv \text{Tr}_F[A_L \rho(t)] \\ &= \text{Tr}_F[e^{iHt} A_L e^{-iHt} \rho(0)]. \end{aligned} \quad (16)$$

We emphasize that expression (14) is designed to provide the steady-state value and not the transients, given our assumption (7).

The two operators  $\rho_S(t)$  and  $A_S(t)$  are subsystem operators. They are simulated in the next section directly, using INFPI, or studied in a perturbative manner, under the Markovian limit, to provide Kinetic-type expressions.

## IV. METHODS

### A. Path-integral simulations

The principles of the INFPI approach have been detailed in Refs. 16 and 17, where it has been adopted for investigating dissipation effects in the nonequilibrium spin-fermion model and charge occupation dynamics in the interacting Anderson model. Other applications include the study of the intrinsic coherence dynamics in a double quantum dot Aharonov-Bohm interferometer,<sup>31</sup> the exploration of relaxation and equilibration dynamics in finite metal grains,<sup>32</sup> and the study of electron-phonon effects in molecular rectifiers.<sup>33</sup>

Here, using INFPI, we can directly simulate both the dynamics of the reduced density matrix  $\rho_S(t)$  [Eq. (5)], and the time evolution of subsystem expectation values, particularly  $A_S(t)$  [Eq. (16)], which can be used to obtain the energy current  $\langle J_L \rangle$ , Eq. (14). In practice, for achieving fast convergence, we have simulated directly the averaged current

$$J = \frac{1}{2}(\langle J_L \rangle - \langle J_R \rangle). \quad (17)$$

The negative sign in front of  $\langle J_R \rangle$  goes back to the sign convention; the current  $\langle J_\nu \rangle$  is defined positive when flowing from the  $\nu$  reservoir, into the junction.

Algorithmic details of the INFPI method were elaborated on in Refs. 9 and 33, thus we only include the main principles here. The algorithm is based on a Trotter breakup of a short-time time evolution operator into two parts: a (simple) time evolution term that depends on the subsystem Hamiltonian, and a term that accommodates the reservoirs Hamiltonians and their interactions with the subsystem. Collecting the contribution of the latter terms along the subsystem path, we construct the so-called ‘‘influence functional’’ (IF), which involves nonlocal dynamical correlations. The IF has an analytical form in some special cases,<sup>18</sup> in the present model its form is only known in the weak-intermediate coupling limit,<sup>8,9</sup> thus we evaluate it numerically by energy-discretizing the Fermi sea.

The main conceptual element behind the INFPI approach is the observation that at finite temperatures and/or nonzero chemical potential bias bath correlations exponentially decay in time, allowing for their truncation beyond a memory time  $\tau_c$ . The dynamics can then be achieved by defining an auxiliary density matrix, or more generally, a subsystem operator

[e.g.,  $A_S(t)$  of Eq. (16)], on the time window  $\tau_c$ . This nonlocal object can be iteratively evolved from the subsystem-bath factorized initial condition, to the present time  $t$ .

Our path-integral method involves three numerical parameters: (i) the number of states used in the discretization of each Fermi sea  $L$ ; (ii) the time step adopted in the Trotter breakup  $\delta t$ ; and (iii) the memory time accounted for  $\tau_c$ , beyond which the IF, accommodating the effect of the reservoirs on the subsystem, is truncated. The convergence of INFPI is verified by confirming that the results are insensitive to the reservoirs discretization, the finiteness of the time step, and the memory size  $\tau_c = N_s \delta t$ , with  $N_s$  as an integer. It should be noted that minimizing the Trotter breakup error, taking  $\delta t \rightarrow 0$ , conflicts with the need to cover the memory time window  $\tau_c$ . Since our computational effort scales as  $d^{2N_s}$ , where  $d$  is the Hilbert space dimensionality of the subsystem, we are practically limited to  $N_s < 10$ . This in turn implies that the time step selected must be *large* enough, so as to cover the characteristic decorrelation time  $\tau_c$  with few ( $N_s$ ) blocks.

### B. Markovian master equation

The dynamics of the model (2), and variants, can be analyzed in the weak subsystem-bath coupling limit under the Markovian approximation to yield quantum mechanical kinetic-type equations.<sup>34</sup> This approach relies on several standard approximations. First, it is based on a second-order perturbation theory expansion of the quantum Liouville equation in the subsystem-bath parameter, and as such it is essentially limited to describe dynamics of subsystems weakly coupled to their environments. Under this approximation, once taking a factorized (subsystem-bath) initial condition, one derives a set of coupled integrodifferential equations for the elements of the (subsystem) RDM. To simplify these equations, the Markovian assumption is invoked, relying on a time-scale separation between the subsystem (slow) and the bath (fast). This step reduces the integrodifferential equations into time-local equations. The result, e.g., the Redfield equation,<sup>35</sup> can be feasibly solved numerically or analytically in the transient regime<sup>36</sup> or in the steady-state limit.<sup>37</sup> In some cases, one may invoke an additional secular approximation, so as to separate the dynamics of the diagonal and off-diagonal elements of the RDM. The secular approximation is typically justified when the energy differences between the subsystem levels ( $\Delta E/\hbar$ ) are large compared to the subsystem relaxation rates.

This standard treatment has been used in many recent works for investigating energy, spin, and charge transfer in open quantum systems.<sup>20,21</sup> Particularly, it has been recently adopted for modeling radiative the energy transfer between metals,<sup>13,28</sup> and for studying charge and energy transfer phenomenology in mesoscopic systems<sup>19,22,24,25</sup> and single molecules.<sup>23,38</sup> It is thus important to test the suitability and accuracy of this common and well-accepted approximate scheme against exact results.

It should be noted that there are numerous flavors for the quantum Kinetic approach. For example, one may go beyond the standard subsystem-bath perturbative treatment (used in this work), by performing a unitary transformation of the Hamiltonian. In the resulting Hamiltonian the perturbative

parameter may effectively include strong subsystem-bath interactions. This idea is employed in, e.g., studies of phonon-assisted electron,<sup>39</sup> exciton,<sup>40</sup> and heat transfer,<sup>41</sup> by adopting the small polaron transformation.<sup>42</sup> Here, we perform the perturbative expansion on the Hamiltonian (2) with  $\alpha$  as the perturbative parameter. For convenience, we refer to the resulting rate equations as ‘‘Markovian master equations,’’ without specifying the perturbative scheme.

Following the steps explained above using the model (2), we find that the probabilities  $P_n$  to occupy the  $|n\rangle$  state of the subsystem  $n = 0, 1$  of energy  $E_n$ , satisfy the master equation

$$\dot{P}_n = \sum_m P_m k_{m \rightarrow n} - P_n \sum_m k_{n \rightarrow m}, \quad (18)$$

where the transition rate from the state  $|m\rangle$  to  $|n\rangle$  ( $m \neq n$  and  $m, n = 0, 1$  here) is additive in the  $L$  and  $R$  reservoirs

$$k_{n \rightarrow m} = k_{n \rightarrow m}^L + k_{n \rightarrow m}^R, \quad (19)$$

due to the linear form of the interaction.<sup>21,43</sup> It should be noted that in the present two-state model one does not need to invoke the secular approximation for deriving (18): Given the structure of the Hamiltonian (2), one immediately obtains from the perturbation expansion time-convolutionless rate equations, where the off-diagonal elements of the reduced density matrix are decoupled from the population dynamics, even beyond second-order perturbation theory.<sup>44</sup>

In the steady state, taking Eq. (14) as a starting point, one can show that in the weak coupling limit and under the Markovian approximation the energy current across the system reduces to<sup>29</sup> ( $\langle J_L \rangle = J$  in the steady state)

$$J = \sum_{m,n} E_{m,n} P_n k_{n \rightarrow m}^L, \quad (20)$$

with  $E_{m,n} = E_m - E_n$ . At the level of the Golden-Rule formula, the transition rates are given by<sup>13</sup>

$$\begin{aligned} k_{n \rightarrow m}^v &= 2\pi \sum_{j,j'} |\alpha_{v,j;j'}|^2 n_F^v(\epsilon_j) [1 - n_F^v(\epsilon_{j'})] \delta(\epsilon_j - \epsilon_{j'} - E_{m,n}) \\ &= 2\pi \int d\epsilon n_F^v(\epsilon) [1 - n_F^v(\epsilon - E_{m,n})] F_v(\epsilon). \\ &= -2\pi n_B^v(E_{m,n}) \int d\epsilon [n_F^v(\epsilon) - n_F^v(\epsilon - E_{m,n})] F_v(\epsilon). \end{aligned} \quad (21)$$

From the last relation we note that the thermal properties of the reservoirs are concealed within both the Fermi-Dirac distribution function  $n_F^v(\epsilon) = [e^{(\epsilon - \mu_v)/T_v} + 1]^{-1}$  and the Bose-Einstein occupation factor  $n_B^v(\epsilon) = [e^{\epsilon/T_v} - 1]^{-1}$ . It is therefore clear that when the integral yields a temperature-independent constant, the statistic of the reservoirs is fully bosonic.<sup>13</sup> The other element in Eq. (21) is a dimensionless interaction term

$$F_v(\epsilon) = |\alpha_v|^2 \rho_v(\epsilon) \rho_v(\epsilon - E_{m,n}), \quad (22)$$

which encloses the properties of the reservoirs, multiplied by the subsystem-bath (energy-independent) couplings  $\alpha_v$ . Once we assume that the density of states is a constant,<sup>45</sup>  $F_v(\epsilon) \approx F_v(\mu_v)$ , the integration in Eq. (21) can be readily performed when the Fermi energies are situated far from the

conduction band edges.<sup>45</sup> Making use of the following relation

$$\int_{-\infty}^{\infty} d\epsilon [n_F^v(\epsilon) - n_F^v(\epsilon - E_{m,n})] = -E_{m,n}, \quad (23)$$

we reach the closed-form expression

$$k_{n \rightarrow m}^v = 2\pi n_B^v(E_{m,n}) E_{m,n} F_v(\mu_v). \quad (24)$$

Note that  $n_B(-E_{m,n}) = -[n_B(E_{m,n}) + 1]$ , thus the excitation and relaxation rates induced by the  $v$  reservoir satisfy the detailed balance relation  $k_{n \rightarrow m}^v/k_{m \rightarrow n}^v = e^{-E_{m,n}/T_v}$ .

Going back to Eq. (2), we recognize that in this two-state model  $E_{1,0} = 2\Delta$ . It is now useful to express the rates in terms of a subsystem-bath interaction parameter

$$\Gamma_F^v(2\Delta) \equiv 2\pi F_v(\mu_v) 2\Delta = 2 \frac{2\Delta}{\pi} [\pi \rho_v(\mu_v) \alpha_v]^2, \quad (25)$$

where we recall that both density of states and the interaction parameter  $\alpha$  are assumed to be energy independent. Using this definition, the excitation and relaxation rate constants reduce to

$$\begin{aligned} k_{1 \rightarrow 0}^v &= \Gamma_F^v(2\Delta) [1 + n_B^v(2\Delta)], \\ k_{0 \rightarrow 1}^v &= \Gamma_F^v(2\Delta) n_B^v(2\Delta). \end{aligned} \quad (26)$$

For simplicity, we do not include below the explicit dependence of  $\Gamma_F^v$  and  $n_B^v$  on energy; both quantities should be evaluated at the subsystem energy gap  $2\Delta$ . We calculate the population of the states in the steady state by putting  $\dot{P}_n = 0$  in Eq. (18). With this at hand, the energy current (20) simplifies to<sup>41</sup>

$$J = 2\Delta \frac{\Gamma_F^L \Gamma_F^R [n_B^L - n_B^R]}{\Gamma_F^L (1 + 2n_B^L) + \Gamma_F^R (1 + 2n_B^R)}. \quad (27)$$

This expression provides the steady-state energy current in the weak coupling limit, under the Markovian approximation.

A more involved, noninteracting blip-approximation (NIBA) type scheme,<sup>1</sup> can be implemented for following the qubit dynamics in the nonequilibrium spin-fermion model.<sup>7</sup> Furthermore, besides the qubit dynamics itself, the heat current can be simulated within the NIBA approximation by extending a generating function technique developed by the authors of Ref. 46 for the study of transport behavior in the nonequilibrium spin-boson model. Here we contain ourselves with the simpler, more standard, and common Markovian master equation, with the objective to provide insight on its applicability and accuracy for the large community adopting it in studies of charge, spin, and energy dynamics in mesoscopic and molecular systems.

## V. RESULTS

We compare INFPI simulations to master equation predictions. Within INFPI, the current is simulated directly using Eqs. (16) and (14), and we show results only in the long time (quasi) steady-state limit. The closed-form master equation expression is given in Eq. (27). Practically, we calculate the current directly from Eq. (20) using the rates (21) since deviations from the wide-band limit may show given the finite value employed here for the bandwidth, for details see the discussion of Fig. 2.

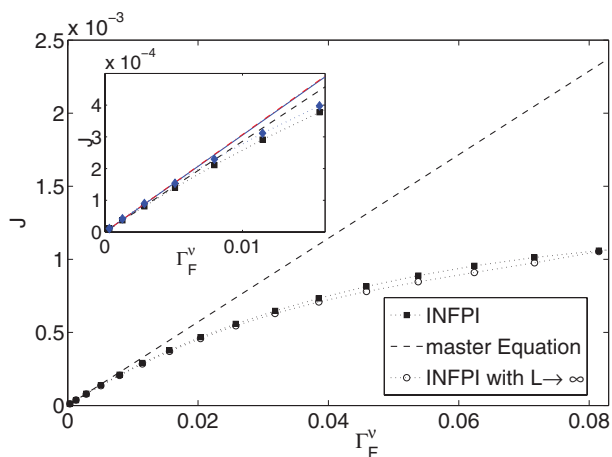


FIG. 2. (Color online) Energy current as a function of metal-qubit coupling parameter  $\Gamma_F^v$  using the bandwidth  $D=2$ ,  $\Delta=0.1$ ,  $T_L=0.4$ , and  $T_R=0.2$ . INFPI numerical parameters are taken as  $\delta t=1$  and  $N_s=9$ . Dashed line: Master equation results. INFPI results appear in symbols,  $\blacksquare$  for  $L=40$  and  $\circ$  when taking the asymptotic  $L \rightarrow \infty$  limit. Inset: Zooming over the small coupling limit; the current linearly scales with  $\Gamma_F^v$ . The inset also displays results using a broader band with  $D=4$ . INFPI results ( $\diamond$ ) are compared to master equation data (full line). The case of  $D=10$  (using master equation) is marked by dashed-dotted line. It practically overlaps with the full line of  $D=4$ .

We use here the following set of parameters: An energy gap  $2\Delta=0.2$  (arbitrary units) for the subsystem, bands extending from zero to  $D=2$  with a flat density of states and a linear dispersion, high enough temperature such that  $T_v \gtrsim \Delta$ , and the equilibrium Fermi energies located at the center of the band. We also define the dimensionless parameter

$$\phi_v = \pi \rho_v \alpha_v, \quad (28)$$

which is varied between 0 and 0.8 here, where convergence is achieved. This choice corresponds to  $0 < \Gamma_F^v < 0.08$  when  $\Delta=0.1$ , see Eq. (25). For this set of model parameters, we have confirmed that selecting  $\delta t=0.8-1.5$  and  $N_s=6-9$  (yielding memory time  $\tau_c \gtrsim 8$ ) provides converging results, see Figs. 5(b), 6(b), and 7(b).

Before turning to simulations, it is important to identify the regime of weak subsystem-bath coupling. It holds when  $\Gamma_F^v/(2\Delta) \ll 1$ , but practically it is enough to demand that  $\Gamma_F^v/(2\Delta) < 0.1$ , with a large subsystem gap relative to the coupling energy. The intermediate limit is defined in the range  $\Gamma_F^v/(2\Delta) \sim 0.1-0.25$ . Now, since  $\Gamma_F^v/(2\Delta) = \frac{2}{\pi} [\pi \rho_v (\mu_v) \alpha_v]^2$ , we can also write these regions using the dimensionless parameter  $\phi_v$ . The relation  $\phi_v \lesssim 0.3$  represents the weak coupling limit,  $0.3 \lesssim \phi_v \lesssim 0.6$  covers the intermediate regime, and  $\phi_v \gtrsim 0.6$  reaches the strong coupling limit. The dimensionless parameter  $\phi_v$  is also related to the scattering phase shift,<sup>47</sup> which should be small at weak coupling. Thus, the weak coupling limit can be also identified when  $\phi_v \sim \tan \phi_v$  is satisfied.

Figure 2 displays the energy current as a function of the interaction energy for a symmetric junction  $\Gamma_F^L = \Gamma_F^R$ . We find that when  $\Gamma_F^v \gtrsim 0.02$ , the master equation-derived energy current overestimates the exact result by more than 10%. In

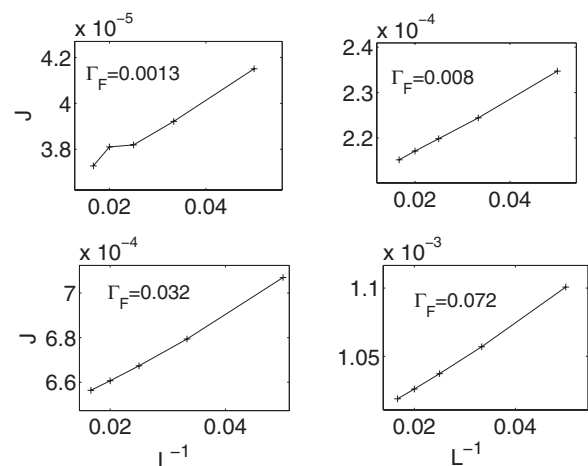


FIG. 3. Converging the data of Fig. 2 to the  $L^{-1} \rightarrow 0$  limit, with the intercept representing the asymptotic result.

the strong coupling limit, the master equation overvalues the correct numbers by a factor of 2. More significantly, this Golden-Rule-based method cannot reproduce the saturation effect of the current with the subsystem-bath interaction parameter, and it wrongly predicts a linear scaling  $J \propto \Gamma_F^v$ . Note that we include INFPI results both for the case of  $L=40$  bath states ( $\square$ ), and in the asymptotic  $L \rightarrow \infty$  limit ( $\circ$ ), obtained by extrapolating the linear  $J$  vs.  $L^{-1}$  curves to  $L^{-1} \rightarrow 0$ , see Fig. 3. We find that this extrapolation affects the results by up to 4% at strong coupling, while the weak coupling values are unaffected. While we do not show transient data for the current, we comment that the steady state has been reached at  $\Delta \times t \sim 50-150$  in the weak coupling limit; it is established much faster,  $\Delta \times t \sim 5-10$  at strong coupling.

The role of the bandwidth is studied in the inset of Fig. 2, where we compare  $D=2$  results to the case of broader bands with  $D=4$ . Since INFPI involves discretized Fermi seas, it is technically difficult to use it for describing broad, yet continuous, bands, as many electronic states should be employed. We thus show results only in the weak coupling limit when broad-band simulations converge. Note that master equation calculations indicate that bands of  $D=4$  practically serve as broad bands (the dashed-dotted line overlaps with full line). We conclude that while the change from  $D=2$  to  $D=4$  does lead to the enhancement of the current by  $\sim 7\%$ , both curves consistently shift and the observed trends are expected to be similar, even at strong coupling, as the relation  $D > \Gamma_F^v$  is maintained.

We correlate transport behavior of the junction with a study of the dissipative dynamics of the spin polarization, as obtained from INFPI, in Fig. 4. We observe weakly damped coherent oscillations in the weak coupling limit when the perturbative master equation well describes the dynamics. These oscillations still survive at intermediate coupling, but at strong coupling the polarization exponentially decays in time (inset). Crucial parameters of the model are the scattering phase shifts  $\delta_{\pm}$ . In equilibrium, the phase shifts are given by<sup>47,48</sup>

$$\tan \delta_{\pm} = \phi_{L,R}. \quad (29)$$

Out-of-equilibrium,  $\Delta\mu \neq 0$ , the phase shifts are *complex* numbers.<sup>48</sup> In the spin-boson model the Kondo dimensionless

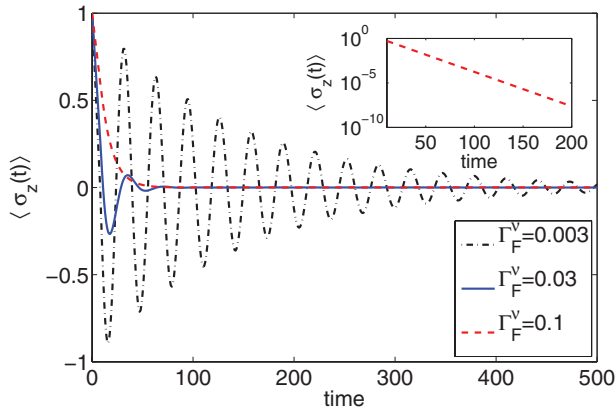


FIG. 4. (Color online) Polarization dynamics at different coupling strengths, for the same set of parameters as in Fig. 2. Results were obtained using INFPI, and they are displayed in the basis in which the Hamiltonian (4) is presented.

dissipation coefficient  $\xi$  represents a characteristic exponent in the system: At zero temperature and zero energy bias the spin displays damped coherent oscillations for  $\xi < 0.5$ , relaxation dynamics between  $0.5 \leq \xi < 1$ , and a localization phase for  $\xi \geq 1$  (Ref. 49). Thus, this parameter controls dissipation-induced phase transitions. In the fermionic analog it can be shown that the characteristic exponent is given by  $\xi = (\delta_+^2 + \delta_-^2)/\pi^2$ , see Ref. 48. Since  $|\delta_{\pm}| \leq \pi/2$ ,  $\xi \leq 1/2$ . Thus, in the spin-fermion model described in this paper the spin cannot manifest the localization behavior, and a large  $\phi$  value brings us to the relaxation scenario, as indeed observed in Fig. 4.

The current-temperature characteristics of the junction are depicted in Figs. 5 through 7, using different coupling strengths. We find that at weak coupling the Markovian master equation very well reproduces the qualitative and quantitative

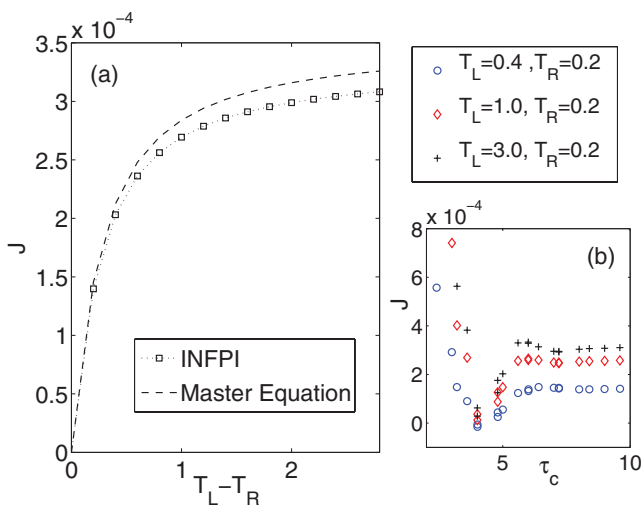


FIG. 5. (Color online) (a) Energy current-temperature characteristics at weak coupling  $\Gamma_F^v = 0.005$  (or equivalently  $\phi_v = 0.2$ ) for the same set of parameters as in Fig. 2. We vary  $T_L$ , but keep  $T_R$  fixed,  $T_R = 0.2$ . (b) Convergence behavior with increasing memory size. Data were produced with three different time steps  $\delta t = 0.8, 1.0$ , and 1.2.

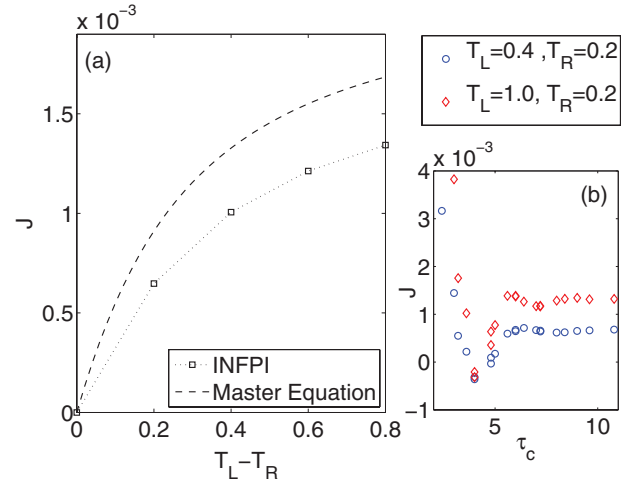


FIG. 6. (Color online) (a) Energy current-temperature characteristics at intermediate coupling,  $\Gamma_F^v = 0.032$  ( $\phi_v = 0.5$ ), for the same set of parameters as in Fig. 2. We vary  $T_L$ , but keep  $T_R$  fixed,  $T_R = 0.2$ . (b) Convergence behavior with increasing memory size. Data were produced with three different time steps  $\delta t = 0.8, 1.0$ , and 1.2.

aspects of the current, even at a large temperature difference, see Fig. 5. The convergence behavior of the INFPI method at different temperature biases is displayed in Fig. 5(b), where we show the energy current as obtained using different memory time  $\tau_c$  and time steps. At intermediate couplings, Fig. 6 shows that the master equation overestimates exact results by up to 25% at large temperature differences. When the subsystem-bath coupling is large, we managed to converge simulations only up to the bias  $T_L - T_R \sim 0.2$ . The Kinetic method now provides values that are a factor of 2 larger than the exact numerical data. It is important to note that the qualitative current-temperature features are correctly reproduced within the Markovian master equation, even at strong coupling.

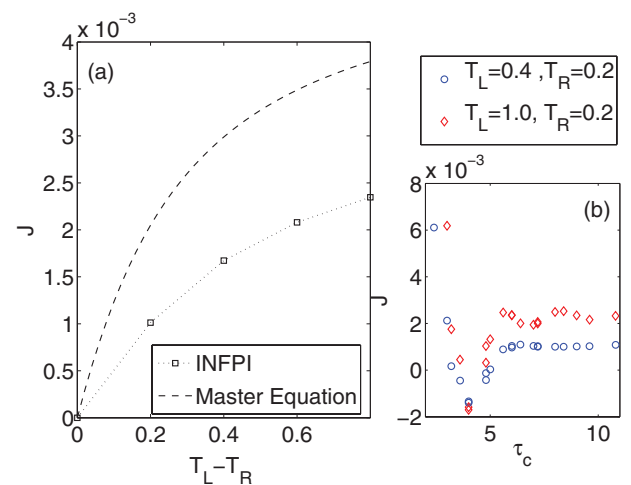


FIG. 7. (Color online) (a) Energy current-temperature characteristics at strong coupling,  $\Gamma_F^v = 0.072$  ( $\phi_v = 0.75$ ), for the same set of parameters as in Fig. 2. We vary  $T_L$ , but keep  $T_R$  fixed,  $T_R = 0.2$ . (b) Convergence behavior with increasing memory size: Results converge only at small bias,  $T_L - T_R < 0.4$ . Data were produced with three different time steps,  $\delta t = 0.8, 1.0$ , and 1.2.

However, if one is interested in quantitative information, master equation can be used in its strict regime of applicability only  $\Gamma_F^v/\Delta \lesssim 0.1$ . The Data in Figs. 5 to 7 are presented for a fixed value of bath states  $L = 40$  since we have confirmed that taking the large- $L$  limit only corrects the current by  $\lesssim 4\%$ , at both low and high temperature biases.

## VI. SUMMARY

We have studied energy transfer between metals mediated by a quantum impurity, using two approaches: Numerically exact path-integral simulations and analytic results from a Golden-Rule-type Markovian master equation treatment. We found that standard master equations fail to reproduce the current-interaction energy characteristics already at intermediate system-bath couplings, as it can only provide a linear enhancement of the current with the subsystem-bath interaction, missing a saturation effect. In contrast, the current-temperature characteristics are produced in a qualitatively correct way by a master equation formalism, though the actual values deviate by 100%, and more, at high temperature biases and at strong coupling.

Our results are beneficial for the critical testing of common master equation techniques. The methods described are also

useful for practically modeling superconducting-based qubit devices.<sup>50</sup> While a master equation treatment offers simple-intuitive expressions that often allow to discern essential transport characteristics, already at intermediate system-bath couplings it may overestimate the current by  $\sim 10\%$ , up to a 100% incorrect enhancement at strong coupling. These deviations are certainly important when a quantitative analysis of device efficiency is performed. In particular, the calculation of energy conversion efficiency in conducting junctions should be done with caution when a master equation is of use.<sup>22,26,51</sup>

In our future work we plan to study the heat current characteristics in the complementary spin-boson type molecular junction model.<sup>41</sup> This could be done by extending the Feynman-Vernon IF expression<sup>52</sup> to describe the evolution of other operators besides the reduced density matrix. Alternatively, one could use the bosonization approach and draw general results for the nonequilibrium spin-boson problem, based on the spin-fermion model calculations presented here.

## ACKNOWLEDGMENT

Support from an NSERC discovery grant is acknowledged.

- 
- <sup>1</sup>A. J. Leggett, S. Chakravarty, A. T. Dorsey, M. P. A. Fisher, A. Garg, and W. Zwerger, *Rev. Mod. Phys.* **59**, 1 (1987).  
<sup>2</sup>U. Weiss, *Quantum Dissipative Systems* (World Scientific, Singapore, 1993).  
<sup>3</sup>J. Gilmore and R. McKenzie, *J. Phys.: Condens. Matter* **17**, 1735 (2005).  
<sup>4</sup>J. Kondo, *Prog. Theor. Phys.* **32**, 37 (1964).  
<sup>5</sup>Y. Makhlin, G. Schon, and A. Shnirman, *Rev. Mod. Phys.* **73**, 357 (2001).  
<sup>6</sup>G. D. Fuchs, G. Burkard, P. V. Klimov, and D. D. Awschalom, *Nat. Phys.* **7**, 789 (2011).  
<sup>7</sup>A. Mitra and A. J. Millis, *Phys. Rev. B* **72**, 121102(R) (2005).  
<sup>8</sup>A. Mitra and A. J. Millis, *Phys. Rev. B* **76**, 085342 (2007).  
<sup>9</sup>D. Segal, D. R. Reichman, and A. J. Millis, *Phys. Rev. B* **76**, 195316 (2007).  
<sup>10</sup>R. M. Lutchyn, L. Cywinski, C. P. Nave, and S. DasSarma, *Phys. Rev. B* **78**, 024508 (2008).  
<sup>11</sup>M. Meschke, W. Guichard, and J. P. Pekola, *Nature (London)* **444**, 187 (2006).  
<sup>12</sup>J. P. Pekola and F. W. J. Hekking, *Phys. Rev. Lett.* **98**, 210604 (2007).  
<sup>13</sup>D. Segal, *Phys. Rev. Lett.* **100**, 105901 (2008).  
<sup>14</sup>T. Ruokola, T. Ojanen, and A.-P. Jauho, *Phys. Rev. B* **79**, 144306 (2009).  
<sup>15</sup>J. Koch, T. M. Yu, J. Gambetta, A. A. Houck, D. I. Schuster, J. Majer, A. Blais, M. H. Devoret, S. M. Girvin, and R. J. Schoelkopf, *Phys. Rev. A* **76**, 042319 (2007).  
<sup>16</sup>D. Segal, A. J. Millis, and D. R. Reichman, *Phys. Rev. B* **82**, 205323 (2010).  
<sup>17</sup>D. Segal, A. J. Millis, and D. R. Reichman, *Phys. Chem. Chem. Phys.* **13**, 14378 (2011).  
<sup>18</sup>N. Makri, *J. Math. Phys.* **36**, 2430 (1995).  
<sup>19</sup>T. Brandes, *Phys. Rep.* **408**, 315 (2005).  
<sup>20</sup>A. Mitra, I. Aleiner, and A. J. Millis, *Phys. Rev. B* **69**, 245302 (2004).  
<sup>21</sup>L.-A. Wu, C. X. Yu, and D. Segal, *Phys. Rev. E* **80**, 041103 (2009).  
<sup>22</sup>G. Schaller, C. Emary, G. Kiesslich, and T. Brandes, *Phys. Rev. B* **84**, 085418 (2011).  
<sup>23</sup>J. Koch, F. von Oppen, Y. Oreg, and E. Sela, *Phys. Rev. B* **70**, 195107 (2004); J. Koch and F. von Oppen, *Phys. Rev. Lett.* **94**, 206804 (2005); J. Koch, M. E. Raikh, and F. von Oppen, *ibid.* **96**, 056803 (2006); J. Koch, M. Semmelhack, F. von Oppen, and A. Nitzan, *Phys. Rev. B* **73**, 155306 (2006).  
<sup>24</sup>T. Ojanen, *Phys. Rev. B* **80**, 180301 (2009).  
<sup>25</sup>T. Ruokola and T. Ojanen, *Phys. Rev. B* **83**, 241404 (2011).  
<sup>26</sup>T. Ruokola and T. Ojanen, *Phys. Rev. B* **86**, 035454 (2012).  
<sup>27</sup>G. Schaller, *Phys. Rev. E* **83**, 031111 (2011).  
<sup>28</sup>P. J. Jones, J. A. M. Huhtamaki, K. Y. Tan, and M. Mottonen, *Phys. Rev. B* **85**, 075413 (2012).  
<sup>29</sup>L.-A. Wu and D. Segal, *J. Phys. A: Math. Theory* **42**, 025302 (2009).  
<sup>30</sup>K. Velizhanin, H. Wang, and M. Thoss, *Chem. Phys. Lett.* **460**, 325 (2008).  
<sup>31</sup>S. Bedkihal and D. Segal, *Phys. Rev. B* **85**, 155324 (2012).  
<sup>32</sup>M. Kulkarni, K. L. Tiwari, and D. Segal, *Phys. Rev. B* **86**, 155424 (2012); *New J. Phys.* **15**, 013014 (2013).  
<sup>33</sup>L. Simine and D. Segal, [arXiv:1302.5761](https://arxiv.org/abs/1302.5761).  
<sup>34</sup>H.-P. Breuer and F. Petruccione, *The Theory of Open Quantum Systems* (Oxford University Press, New York, 2002).  
<sup>35</sup>A. G. Redfield, *IBM J. Res. Dev.* **1**, 19 (1957); *Appl. Magn. Reson.* **1**, 1 (1965).

- <sup>36</sup>W. T. Pollard, A. K. Felts, and R. A. Friesner, *Adv. Chem. Phys.* **93**, 77 (1996).
- <sup>37</sup>D. Segal, A. Nitzan, W. B. Davis, M. R. Wasielewsky, and M. A. Ratner, *J. Phys. Chem. B* **104**, 3817 (2000).
- <sup>38</sup>L. Simine and D. Segal, *Phys. Chem. Chem. Phys.* **14**, 13820 (2012).
- <sup>39</sup>D. Segal and A. Nitzan, *Chem. Phys.* **281**, 235 (2002).
- <sup>40</sup>A. Kolli, A. Nazir, and A. Olaya-Castro, *J. Chem. Phys.* **135**, 154112 (2011).
- <sup>41</sup>D. Segal and A. Nitzan, *Phys. Rev. Lett.* **94**, 034301 (2005); *J. Chem. Phys.* **122**, 194704 (2005).
- <sup>42</sup>G. D. Mahan, *Many Particle Physics* (Plenum, New York, 2000).
- <sup>43</sup>D. Segal, *Phys. Rev. B* **73**, 205415 (2006).
- <sup>44</sup>B. B. Laird, J. Budimir, and J. L. Skinner, *J. Chem. Phys.* **94**, 4391 (1991).
- <sup>45</sup>B. N. J. Persson and H. Ueba, *Phys. Rev. B* **76**, 125401 (2007).
- <sup>46</sup>L. Nicolin and D. Segal, *J. Chem. Phys.* **135**, 164106 (2011).
- <sup>47</sup>B. Roulet, J. Gavoret, and P. Nozieres, *Phys. Rev.* **178**, 1072 (1969); P. Nozieres and C. T. D. Dominicis, *ibid.* **178**, 1097 (1969).
- <sup>48</sup>T.-K. Ng, *Phys. Rev. B* **54**, 5814 (1996).
- <sup>49</sup>K. L. Hur, *Understanding Quantum Phase Transitions* (Taylor and Francis, Boca Raton, FL, 2010).
- <sup>50</sup>M. M. J. T. Muhonen and J. P. Pekola, *Rep. Prog. Phys.* **75**, 046501 (2012).
- <sup>51</sup>M. Esposito, K. Lindenberg, and C. V. den Broeck, *Euro. Phys. Lett.* **85**, 60010 (2009).
- <sup>52</sup>R. P. Feynman and A. R. Hibbs, *Quantum Mechanics and Path Integrals* (McGraw-Hill, New York, 1965).